Endothelin receptor antagonism prevents hypoxia-induced mortality and morbidity in a mouse model of sickle-cell disease

Nathalie Sabaa,[1,2] Lucia de Franceschi,[3] Philippe Bonnin,[1,4,5] Yves Castier,[1] Giorgio Malpeli,[6] Haythem Debbabi,[4] Ariane Galaup,[7,8] Micheline Maier-Redelsperger,[9] Sophie Vandermeersch,[2] Aldo Scarpa,[6] Anne Janin,[10,11] Bernard Levy,[1,4,5] Robert Girot,[9] Yves Beuzard,[11] Christophe Leboeuf,[10,11] Annie Henri,[11] Stéphane Germain,[7,8,12] Jean-Claude Dussaule,[2] and Pierre-Louis Tharaux[1,9]

[1]Cardiovascular Research Center Lariboisière, INSERM U689, Paris, France. [2]INSERM U702, Paris, France. [3]Department of Clinical and Experimental Medicine, Section of Internal Medicine, University of Verona, Verona, Italy. [4]Physiologie-Explorations Fonctionnelles, Hôpital Lariboisière, Assistance Publique-Hôpitaux de Paris, Paris, France. [5]Université Denis Diderot, Paris 7, Paris, France. [6]Department of Pathology, Section of Anatomic Pathology, University of Verona, Verona, Italy. [7]INSERM U833, Paris, France. [8]Collège de France, Paris, France. [9]Service d'Hématologie Biologique, Hôpital Tenon, Assistance Publique-Hôpitaux de Paris, Paris, France. [10]Université Paris Diderot-Paris 7, Institut Universitaire d'Hématologie, Hôpital Saint Louis, Paris, France. [11]INSERM U733, Paris, France. [12]Service d'Hématologie Biologique A, Hôpital Européen Georges Pompidou, Assistance Publique-Hôpitaux de Paris, Paris, France.

Patients with sickle-cell disease (SCD) suffer from tissue damage and life-threatening complications caused by vasoocclusive crisis (VOC). Endothelin receptors (ETRs) are mediators of one of the most potent vasoconstrictor pathways in mammals, but the relationship between vasoconstriction and VOC is not well understood. We report here that pharmacological inhibition of ETRs prevented hypoxia-induced acute VOC and organ damage in a mouse model of SCD. An in vivo ultrasonographic study of renal hemodynamics showed a substantial increase in endothelin-mediated vascular resistance during hypoxia/reoxygenation-induced VOC. This increase was reversed by administration of the dual ETR antagonist (ETRA) bosentan, which had pleiotropic beneficial effects in vivo. It prevented renal and pulmonary microvascular congestion, systemic inflammation, dense rbc formation, and infiltration of activated neutrophils into tissues with subsequent nitrative stress. Bosentan also prevented death of sickle-cell mice exposed to a severe hypoxic challenge. These findings in mice suggest that ETRA could be a potential new therapy for SCD, as it may prevent acute VOC and limit organ damage in sickle-cell patients.

Introduction

Painful vasoocclusive crisis (VOC) is one of the major and specific manifestations of sickle-cell disease (SCD). VOC is a complex process involving hemoglobin S polymer formation and poorly deformable dense rbcs, leading to vasoocclusions of capillaries and postcapillary venules due to activated endothelium entrapping hyperadhesive sickle rbcs, reticulocytes, and leukocytes (1, 2). These multiple local ischemic events cause tissue damage and life-threatening complications (1, 2). We hypothesized that this complex scenario is worsened by vessel contraction. Endothelin-1 (ET-1) is a potent vasoactive peptide and is released by activated endothelial (3, 4) and nonendothelial (5, 6) cells after local tissue hypoxia and low NO availability. In SCD, plasma concentrations of endothelin and other endothelial markers have been reported to be abnormally high (7–9). We have recently shown that the difference between urinary ET-1 concentrations in SCD and in controls was greater than the difference in plasma ET-1 concentrations, suggesting high local renal production of ET-1 in SCD patients (10). However, the pathophysiological relevance and biological effects of ET-1 in SCD in vivo are unknown. Increased plasma and urinary levels of ET-1 in SCD may be late events related to hypoxia- or inflammation-induced cell activation, damage, and/or death rather than being directly involved in pathophysiological events in acute VOC. Consequently, it would be useful to determine ET-1 concentrations in damaged tissues and conduct functional studies of ET receptors (ETRs) in vivo. In SCD, there are contrasting perfusion profiles in the circulatory system: hypoperfusion in microcirculatory beds occluded by sickled, dense erythrocytes and hyperperfusion in the systemic macrocirculation associated with various regional vascular circuits. Kidneys and lungs are particularly vulnerable to acute VOC because of their anatomical features (11–13). The renal medulla has substantial epithelial metabolic activity, with high oxygen demand, hyperosmolarity, and low pH and is thus very susceptible to hypoxia. Damage to the renal medulla is a common feature of SCD patients (14, 15). The extremely large capillary network of the pulmonary circulation is a low pressure system which is frequently subjected to acute ischemic insults, leading to acute pulmonary hypertension (16).

We assessed the in vivo effects of the dual endothelin receptor antagonist (ETRA) bosentan (17) on resistive microvascular beds and in particular in the renal vasculature of transgenic mice expressing human hemoglobin SAD ($\alpha 2\beta 2^{SAD}$) (18). SAD mice, used as models for SCD, have the advantage of suffering experi-

Nonstandard abbreviations used: BFV, blood-flow volume; CO, cardiac output; ET-1, endothelin-1; ETB, ET-1 type B receptor; ETR, endothelin receptor; ETRA, ETR antagonist; H/R, hypoxia/reoxygenation; MPO, myeloperoxidase; RC, repeatability coefficient; SCD, sickle-cell disease; VOC, vasoocclusive crisis.

Conflict of interest: The authors have declared that no conflict of interest exists.

Citation for this article: *J. Clin. Invest.* **118**:1924–1933 (2008). doi:10.1172/JCI33308.

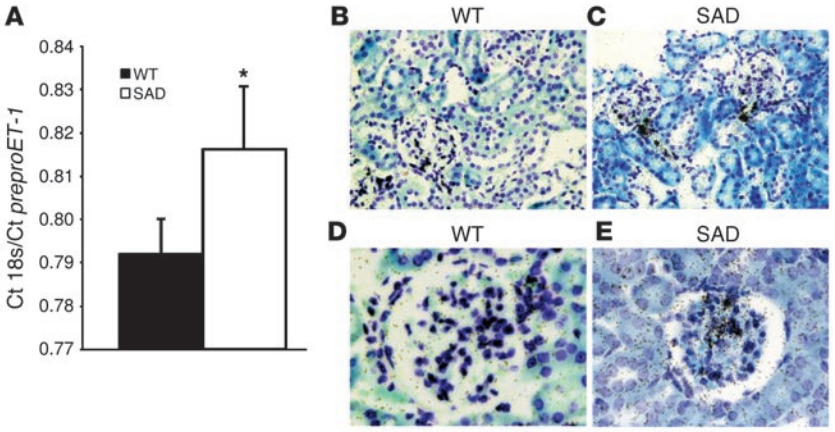

Figure 1
PreproET-1 mRNA levels are higher in sickle-cell mice than in WT mice at steady state. (**A**) Real-time RT-PCR analysis of *preproET-1* from kidneys of C57BL/6J (WT) and SAD mice at steady state (normoxia). $n = 5$ to 7 animals per condition. *$P < 0.05$ versus WT. (**B**–**E**) In situ hybridization for *preproET-1* mRNA in kidneys from WT and SAD mice in steady state. *PreproET-1* mRNA in small vessels is restricted to endothelial cells in the kidney cortex of (**B**) WT and (**C**) SAD mice. *PreproET-1* mRNA is substantially more abundant in (**C**) afferent arterioles and (**E**) glomerular capillaries in SAD mice than in (**B** and **D**) WT mice. Original magnification, ×400 (**B** and **C**); ×600 (**D** and **E**).

mental acute vasoocclusive events when subjected to controlled hypoxia/reoxygenation (H/R) (19); H/R induces lung injury in these mice, closely mimicking the vasoocclusive pathology of patients with SCD (19, 20). We evaluated the effects of H/R in the kidney in the same model of acute VOC and tested to determine whether ETR antagonism prevents hypoxia-induced sickle-cell–related organ damage. We also confirmed the presence of ETR type B (ETB) on mouse red cells and evaluated the effects of ETR antagonism on rbc dehydration in vivo. Note that the stimulation of the Gardos channel pathway by ET-1 in isolated human and mouse rbcs has been reported previously. Indeed, the Gardos channel cascade that induces loss of potassium (K^+) and water (21–23) contributes to generation of dense rbcs that is thought to play an important role in the pathophysiology of SCD.

We found that ETRA treatment specifically protected SAD mice against systemic and tissue inflammation, kidney and lung damage, and death from experimental acute SCD events.

Results

Production of preproET-1 mRNA in kidney. Levels of *preproET-1* mRNA in kidney were higher in SAD mice than in WT mice at steady state (Figure 1A). The mRNA in SAD mice was restricted to the endothelial cells of the kidneys (Figure 1, C and E) and the lungs (not shown), indicating an abnormal phenotype of the endothelium in this mouse model.

Acute endothelin receptor blockade restores renal blood flow after H/R. We investigated the role of ETR-mediated vasoconstriction in the increase in renal vascular resistance during H/R-induced acute VOC. To this end, we assessed cardiac output (CO) and renal blood flow velocity at steady state (normoxia) and during H/R-induced VOC, with or without acute bosentan treatment.

At steady state, ultrasonography-Doppler measurement of CO and blood flow velocity in the renal arteries showed no significant differences between normal and SAD mice (Figure 2, A and B). In contrast, H/R induced a significant decrease in mean renal blood velocities in SAD mice ($P < 0.01$; Figure 2, B and C, and Supplemental Video 1; supplemental material available online with this article; doi:10.1172/JCI33308DS1). The magnitude of renal perfusion impairment exceeded the diminution in CO, and there was no effect on systolic blood pressure (not shown). This suggests that the substantial increase in renal vascular resistance was supported by the large fall in end-diastolic velocities and time-averaged mean blood velocities in untreated SAD mice (Figure 2, B and C, and Supplemental Video 1). We then infused SAD and WT mice with either bosentan or vehicle alone. In SAD mice, bosentan restored 50% of the fall in renal blood velocities within 10 minutes, implicating ET-1–mediated vasoconstriction in H/R-induced acute events ($P < 0.01$ vs. before bosentan infusion) (Figure 2, B and C, and Supplemental Video 1). In contrast, acute infusion of the calcium channel blocker nicardipine failed to promote a significant increase in mean renal blood flow velocity in SAD animals (6.5 ± 0.73, 6.8 ± 1.0, and 5.4 ± 0.6 cm/s at baseline after H/R and 5 and 10 minutes after nicardipine infusion, respectively; NS versus before nicardipine infusion).

Bosentan prevents sickle-cell–related vasoocclusive events: hemodynamic and histopathological studies. Administration of bosentan for 14 days prevented H/R-induced alterations in renal blood flow in SAD mice. The cardiac and renal hemodynamics of these mice, insensitive to H/R, were similar to those observed in WT mice (Figure 2, D and E).

Given the substantial effect of bosentan on renal hemodynamics, we sought to determine the preventive effects of bosentan on renal and lung pathology as well as effects on other cellular targets for ET-1, including rbcs and leukocytes, that harbor ETRs.

SAD mice exposed to H/R have kidney and lung abnormalities similar to those associated with acute sickle-cell vasoocclusive events. Histological analysis of the kidneys of H/R-exposed WT mice showed no injury (Figure 3A), whereas SAD mice had marked congestion in peritubular capillaries and glomerular abnormalities. Cortical peritubular capillaries and capillaries in the medulla were all substantially congested due to entrapment of rbcs (Figure 3A). Glomeruli were also highly congested and had enlarged capillary loops (Figure 3A and Supplemental Figure 1). These findings are similar to histopathological findings in other sickle-cell mouse models of renal ischemia (24) and to human SCD kidney abnormalities (25). Lungs from H/R SAD mice had substantial focal vascular congestion, constriction, generation of thrombi, and mononuclear infiltration into the tissue as previously described (20) (Figure 3B and Supplemental Table 1).

PreproET-1 mRNA was more abundant in SAD than WT mouse kidneys, and bosentan prevented the H/R-induced increase in renal vascular resistance, so we investigated whether ETR antagonism protects kidneys and lungs from acute vasoocclusive events in SAD mice. We determined the proportion of congestive glomeruli per kidney slice and the rbc content per glomerulus assessed by image analysis of the area occupied by rbcs in WT and SAD mice at steady state and after 18 hours hypoxia with 2 hours reoxygenation follow-

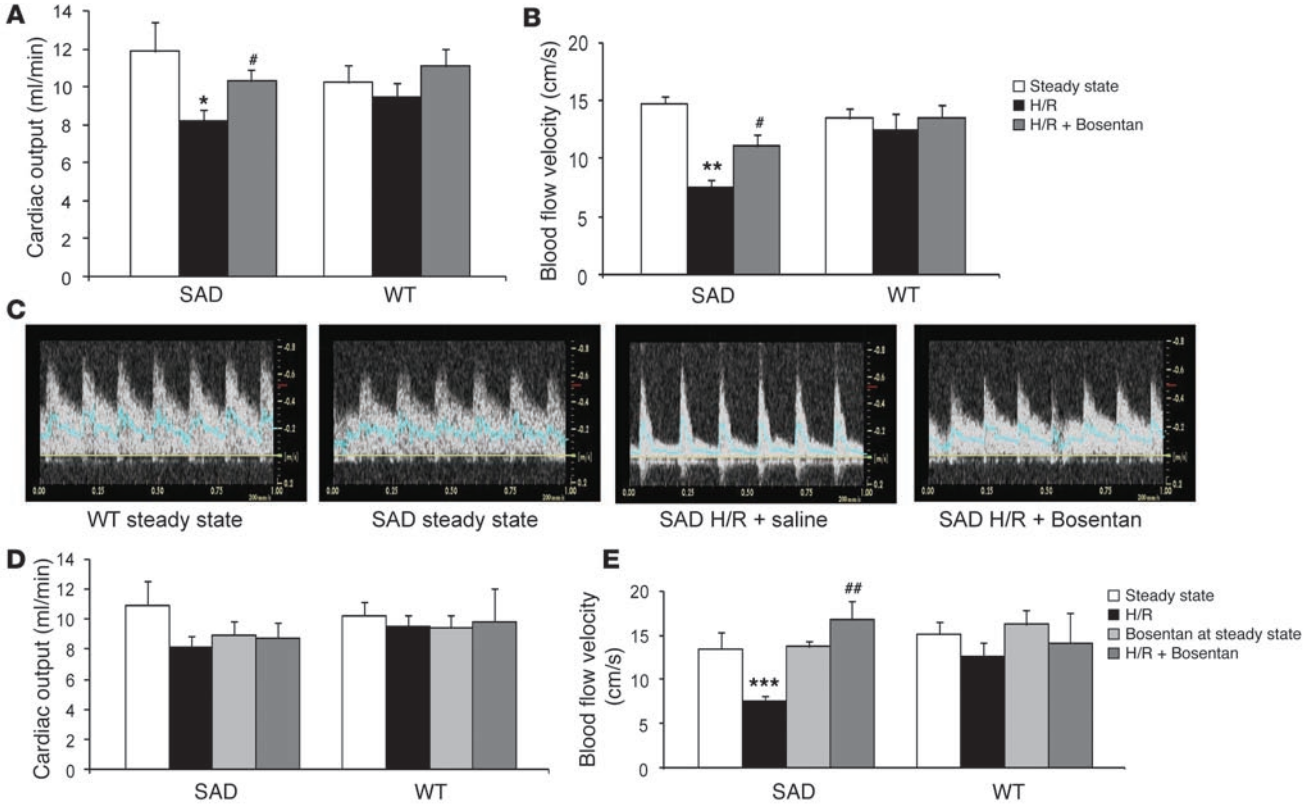

Figure 2

ETRA reverses and prevents the fall in renal blood flow velocity (RBF) in SAD mice. (**A**–**C**) Reversal of low renal perfusion in sickle mice by infusion of bosentan. Echo-Doppler measurements of (**A**) CO and (**B**) RBF velocity in the renal artery at steady state (white bars) and after H/R in SAD and WT mice before (black bars) and 10 minutes after infusion of bosentan (gray bars). H/R-induced vasoocclusive (VOC) events were associated with blunted CO and significant decreases in mean RBF velocity in SAD mice only. Acute infusion of bosentan restored 50% of the initial loss in RBF velocity within 10 minutes, whereas saline had no effect (not shown). $n = 13$. $^{*}P < 0.05$ versus SAD at steady state; $^{**}P < 0.01$ versus SAD at steady state; $^{\#}P < 0.05$ versus SAD before bosentan infusion. (**C**) Representative RBF waveforms in WT and SAD mice at steady state and after H/R followed by acute infusion of saline or bosentan. End-diastolic and time-averaged mean velocities were lower in saline-treated SAD mice after H/R than in normoxic WT and SAD mice. Acute ETRA restored end-diastolic and time-averaged mean velocities. (**D** and **E**) Prevention of H/R-induced renal hypoperfusion in SAD mice treated for 2 weeks with bosentan. (**D**) CO and (**E**) mean RBF velocity were unchanged in bosentan-treated SAD mice, whereas mean RBF velocity decreased by 50% in vehicle-treated SAD mice. All data are means ± SEM from $n = 2$ experiments. $n > 10$. $^{***}P < 0.001$ versus SAD at steady state; $^{\#\#}P < 0.01$ versus vehicle-treated SAD in H/R.

ing 8 days of bosentan or placebo administration. There was no significant change in the proportion of congested glomeruli or in rbc area per glomerulus in WT mice. In placebo-treated SAD mice, the rbc area per glomerulus was larger than that in WT mice (165% of the WT value) ($P < 0.001$). In bosentan-treated SAD mice, however, this difference was much smaller (125% of the WT value) ($P < 0.01$ versus vehicle-treated SAD), indicating that bosentan inhibited congestion in peritubular capillaries and glomeruli (Supplemental Figure 1, A and B) and entrapment of sickled rbcs. Accordingly, the overall proportion of histologically congested glomeruli was substantially reduced by ETRA (Supplemental Figure 1C).

We also found that lungs from H/R SAD mice treated with bosentan had less vascular congestion, constriction, and thrombi formation as well as a milder inflammatory response than those of untreated mice (e.g., less mucus filling the bronchi and less inflammatory cellular infiltration) (Figure 3B and Supplemental Table 1).

The ETRA prevents ET-1–induced in vitro activation of the Ca^{2+}-activated K^+ channel and affects hypoxia-induced in vivo formation of dense red cells in SAD mice. ETB has been described to be present in erythroid cells (21, 23). We evaluated ETB protein abundance in mouse red cells. ETB is present and similarly abundant in WT and SAD mouse red cells (Supplemental Figure 2). We measured the in vitro Gardos channel activity in rbcs from WT and SAD mice in the presence of ET-1, with and without bosentan. Bosentan completely prevented in vitro ET-1–induced Gardos channel activation in rbcs from both WT and SAD mice (Figure 4A). The combined action of 2 rbc membrane cation transport systems — the K-Cl cotransporter and the Gardos channel — contributes to the generation of dense sickle red cells, so we evaluated the effects of bosentan in vivo on the rbc density profile and K^+ content in both these mouse strains under normoxic and under H/R conditions. (Figure 4, B and C). Both rbc K^+ content and density profiles differed significantly between the 2 mouse strains under normoxic conditions, and the difference was exacerbated after H/R. However, rbc K^+ content was higher and rbc density lower in SAD mice exposed to H/R and treated with bosentan than in vehicle-treated SAD mice under H/R conditions. These findings suggest that bosentan prevents the ET-1–sensitive part of the hypoxia-induced activation of Gardos channels.

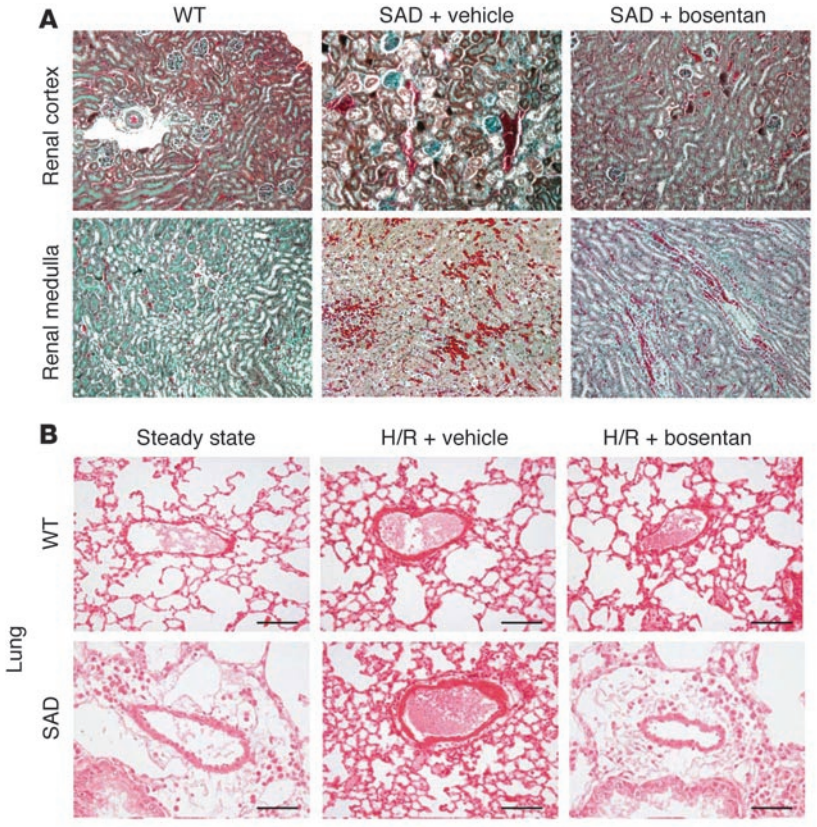

Figure 3
Profound vascular congestion as a result of H/R-induced vasoocclusive events in kidneys and lungs from sickle SAD mice. (**A**) Vehicle-treated sickle SAD mice had substantial vascular congestion in glomeruli, arterioles, and capillaries in the renal cortex (top) and the renal medulla (bottom). This was less frequently observed in glomeruli, arterioles, and capillaries in bosentan-treated sickle SAD mice. (**B**) Representative H&E staining showing alleviation of pulmonary vascular congestion and inflammatory infiltration in bosentan-treated hypoxic sickle SAD mice. Original magnification, ×100 (**A**); ×250 (**B**).

Endothelin receptors contribute to H/R-induced neutrophil recruitment. Hyperleukocytosis and high neutrophil counts are independent predictors of adverse outcome in SCD (26). Human and mouse neutrophils express ETRs on their surfaces, but the role of ETRs has not been completely defined (27). We monitored circulating levels of neutrophils at steady state (normoxia) and after experimental acute VOC in SAD and WT mice. Blood neutrophil counts in SAD mice were significantly higher after 48 hours under hypoxic conditions than under steady state conditions ($P < 0.01$) (Table 1). ETR blockade fully prevented the H/R-induced high neutrophil count in SAD mice and indeed reduced the count to below that in SAD animals at steady state ($P < 0.01$) (Table 1). The neutrophil count in WT mice was increased 2-fold by H/R; this increase was only one third of that in SAD animals. Thus, in WT animals, ETR blockade also prevented systemic mobilization of neutrophils.

Bosentan inhibits neutrophil migration to the kidney and to the bronchoalveolar space in SAD mice. Polymorphonuclear neutrophil recruitment plays a key role in various models of ischemia-reperfusion damage, as it does in sickle-cell–related acute VOC (28). Accordingly, total leukocyte (Figure 5A) and neutrophil counts (Figure 5B) were higher in bronchoalveolar lavage samples from SAD mice under H/R conditions than those at steady state. The increase in

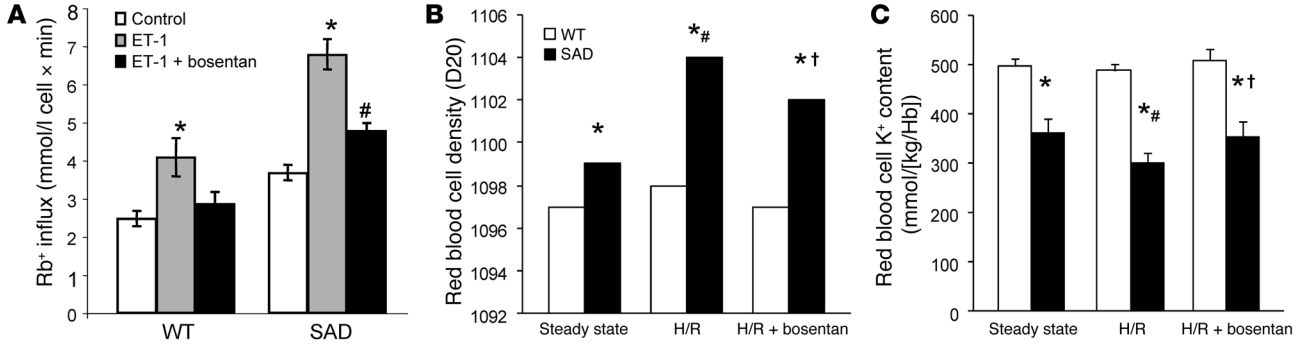

Figure 4
Bosentan prevents in vitro ET-1 activation of the Gardos channel. (**A**) In vitro rubidium (Rb^+) influx (mmol/l cell × min) in WT and SAD mouse rbcs in the presence of ET-1 with or without pretreatment with bosentan. $^*P < 0.05$ versus control Rb^+ influx; $^{\#}P < 0.05$ versus ET-1–treated rbcs. (**B**) In vivo effects of 2-week administration of bosentan on density and (**C**) K^+ content in WT and SAD mouse rbcs. $^*P < 0.05$ versus WT mice; $^{\#}P < 0.05$ versus SAD mice at steady state; $^{\dagger}P < 0.05$ versus vehicle-treated SAD mice; $n = 6$.

Table 1
In vivo effects of bosentan on reticulocyte and neutrophil blood counts in WT and SAD mice exposed to hypoxia

	WT (*n* = 6)	WT H/R (*n* = 6)	WT H/R + bosentan (*n* = 6)	SAD (*n* = 6)	SAD H/R (*n* = 6)	SAD H/R + bosentan (*n* = 6)
Hematocrit (%)	44.5 ± 1.0	45.1 ± 0.8	44.8 ± 0.4	43.9 ± 0.2	42.7 ± 1.3	43.2 ± 0.6
Hemoglobin (g/dk)	13.9 ± 0.8	14.2 ± 0.6	14.6 ± 0.3	13.1 ± 0.5	12.5 ± 0.9	13.3 ± 1.1
Reticulocytes (%)	4.5 ± 1.2	6.1 ± 0.8	5.9 ± 0.7	5.3 ± 0.4	6.2 ± 1.2	6.8 ± 1.5
Neutrophils (cells/μl)	862.7 ± 54	1821 ± 266[A]	827 ± 133[B]	2527 ± 229	5681 ± 811[C]	1321 ± 446[D]

The mice were exposed to hypoxic conditions (8% oxygen) for 46 hours. [A]$P < 0.05$ versus steady state. [B]$P < 0.05$ versus vehicle-treated mice. [C]$P < 0.01$ versus steady state. [D]$P < 0.01$ versus vehicle-treated mice.

cell counts in SAD mice under H/R conditions was reduced by bosentan treatment ($P < 0.05$).

Myeloperoxidase (MPO) activity is a sensitive index of polymorphonuclear neutrophil activation, inducing substantial oxidative stress and thus promoting ischemia/reperfusion injuries (28). Exposure to H/R resulted in high renal and lung MPO activity in SAD mice. Treatment with bosentan starting 8 days before H/R resulted in significantly lower MPO activity in these 2 tissues in SAD mice ($P < 0.05$; Figure 6, A and B), indicating that bosentan is antiinflammatory in the context of experimental VOC.

Endothelin receptor antagonism prevents increased nitrative stress. Changes in systemic and local inflammation accompanied changes in MPO activity in kidneys and lungs from SAD mice (Figure 6, A and B). $NO^{\bullet}$, $O_2^{\bullet -}$, and 3-nitrotyrosine, markers of peroxynitrite- and $NO_2^{\bullet}$-induced nitration of proteins (29, 30), are abundantly generated in sickle-cell mouse kidneys (31, 32). We evaluated the effects of ETR blockade on nitrative stress during acute VOC by assessing nitration of renal tissues in SAD and WT mice. Immunostaining for nitrotyrosine was substantially stronger in SAD mice under H/R conditions than in WT animals under H/R conditions and in SAD and WT mice at steady state (Figure 6, C–E). H/R-induced nitrative stress in the renal cortex in SAD mice was reduced by preventive treatment with bosentan (Figure 6F), and the effect of bosentan was even more evident in the kidney medulla (Figure 6, G and H).

Bosentan protects against H/R vasoocclusive events–related lethality. SAD mice were subjected to very severe, life-threatening H/R exposure (10 hours in a 6% O_2 atmosphere), previously shown to be lethal for SAD mice. Bosentan treatment completely protected these mice from death (0% mortality versus 83% mortality for SAD mice not receiving bosentan) ($P < 0.001$; Figure 6I). None of the bosentan-treated SAD mice died at any time during the experiment, indicating that the effect was durable. No WT mice (whether or not treated with bosentan) died, indicating that death was specifically related to the sickle-cell phenotype.

Discussion

We report that ETR inactivation in a mouse model leads to reversal or prevention of vasoocclusive events, including tissue damage, rbc dehydration, leukocyte recruitment, infiltration of organs with activated neutrophils, nitrative stress, and death. Furthermore, this study is the first, to our knowledge, to demonstrate a rapidly reversible vasospastic component in SCD.

ET-1 levels are abnormally high in plasma and urine from sickle-cell patients (7–10). However, ETRs have very high affinity for ET-1 (in the picomolar range) and ET-1 has local cellular actions, so its production in tissue and its activity may well be more relevant than circulating peptide levels as markers. Therefore, we hypothesized that the *preproET-1* gene is upregulated in 2 organs, the kidney and the lung, in which acute and chronic injuries are major factors of poor prognosis for SCD (33–35). We found that ET-1 is produced at a higher level in the renal and pulmonary microvasculature of SAD mice than WT mice at steady state, consistent with the abnormally high systemic ET-1 levels in sera from SCD patients. ET-1 synthesis has been demonstrated in renal tubules under ischemic conditions (5) and in leukocytes (36). However, in SAD mice, we detected high levels of ET-1 mRNA but only in the capillary and arteriolar endothelium; ET-1 mRNA was scarce in or absent from kidney epithelial cells, lung epithelial cells, and infiltrating leukocytes.

Stimuli for ET-1 gene upregulation have not been analyzed. In acute VOC, sudden falls in blood flow and shear stress may substantially alter endothelial production of NO, a potent inhibitor of ET-1 synthesis and of its vasoconstrictive effect (37). Patho-

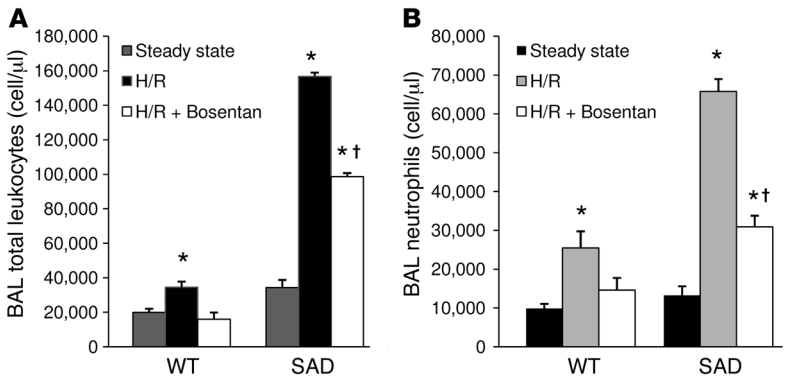

Figure 5
The ETRA bosentan prevents systemic and local inflammation in SAD mice. (**A**) Effect of orally administered bosentan on total leukocyte and (**B**) neutrophil alveolar infiltration in H/R-challenged WT and SAD mice. *$P < 0.05$ versus steady state; †$P < 0.05$ versus vehicle-treated mice.

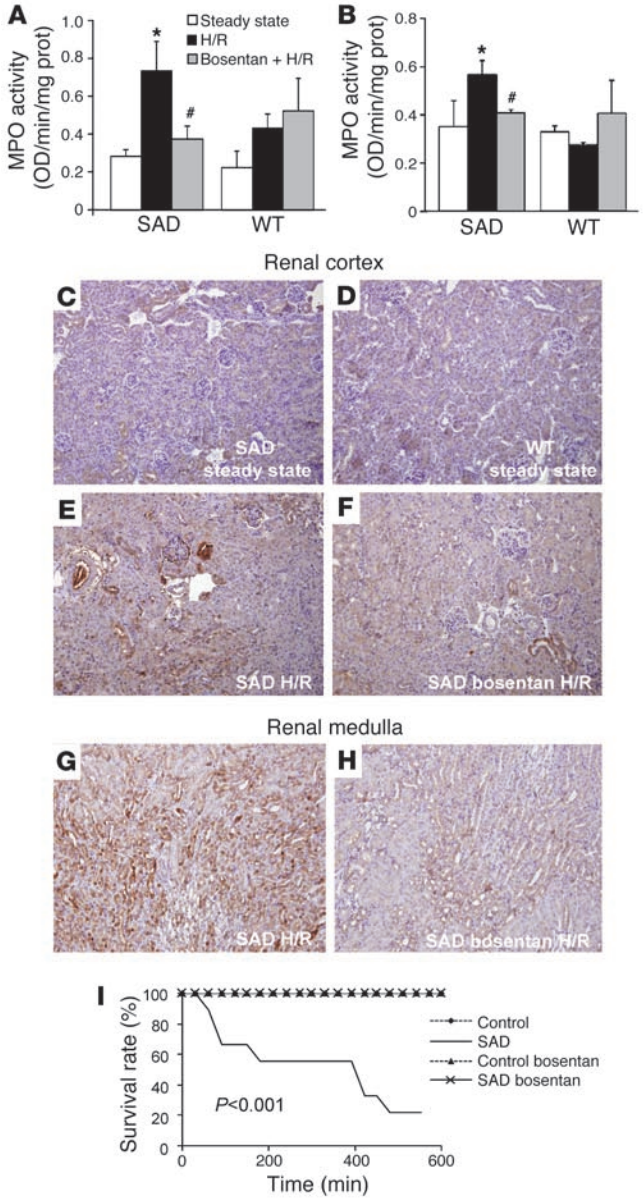

Figure 6
Bosentan prevents increased renal and lung MPO activity, peroxynitrite-induced protein tyrosine nitration in the kidneys, and severe hypoxia–induced death. MPO activity in (**A**) kidneys and (**B**) lungs of WT and SAD mice at steady state and after 18-hour exposure to H/R. $^{*}P < 0.05$ vs. SAD at steady state; $^{\#}P < 0.05$ vs. SAD in H/R. (**C**–**H**) Anti-nitrotyrosine staining of kidney sections is strong in SAD mice in the (**E**) renal cortex and, to an even greater extent, in the (**G**) renal medulla under H/R conditions. (**F** and **H**) Bosentan administration before H/R prevented protein tyrosine nitration in these 2 renal compartments. Original magnification, ×100. (**I**) Endothelin receptor antagonism with bosentan protects SAD mice from death due to severe VOC after exposure to a 6% O_2 atmosphere for 10 hours. Survival curves for vehicle-treated SAD mice are significantly different ($P < 0.001$) from those for bosentan-treated SAD mice and WT controls. n = 8–12 mice per group.

physiological conditions associated with SCD, including diminished bioavailability of NO (32, 38) due to cell-free hemoglobin (39), increased oxidative stress (40), local hypoxia, and cytokine release, may promote activation of endothelial ET-1 production with unbalanced and excessive ET-1–mediated vasoconstriction (41, 42). SAD mice do not display a hemolytic anemia as severe as that observed in most human sickle subjects; this suggests that the shortfall in NO due to cell-free hemoglobin or release of erythrocyte arginase may not be as severe in SAD mice as in patients. This may explain in part why SAD mice experience little spontaneous VOC without a hypoxic challenge. Nevertheless, NO administration has been shown to inhibit VOC-induced lung damage in the same model of H/R-induced VOC (20, 43). These various observations suggest that an imbalance between ET-1 and NO plays a critical role in SCD. They also indicate that marked hemolysis is not required to activate the pathophysiological activities of ET receptors. Our findings suggest that therapeutic targeting of ETR should be beneficial. For instance, SAD mice chronically treated with bosentan did not display significant systemic or regional hemodynamic changes at steady state and did not show any signs of desensitization to protection against the effects of VOC. From a practical point of view, ETRAs already marketed for other medical indications may be useful for prevention of or therapy for VOC.

We also describe what we believe is a novel paradigm for SCD. We used a noninvasive method to measure renal blood flow velocity in the whole kidney; we show (for the first time, to our knowledge) that up to 50% of the fall in renal blood flow induced by experimental VOC is reversed within minutes by acute ETR antagonism. The fast kinetics of this reversal suggest that only SAD but not WT mice suffered substantial renal vasoconstriction, aggravating blood cell entrapment. However, the remaining half of the H/R-induced fall in renal blood flow velocity was only slowly reversible (within 4 to 5 hours under normoxic conditions). This suggests that there was an additional vasoconstrictive effect or, more likely, a partially persistent microvascular obstruction by entrapped dense sickle cells and leukocytes; this interpretation was supported by histopathological observations. Bosentan treatment led to rapid reversal of the VOC-induced reduction of pulmonary blood flow and microvascular congestion and prevented death. It is therefore plausible that the pathophysiology in the pulmonary vasculature was similar to that described for the renal vasculature.

Interestingly, reduction of VOC-induced hypoperfusion and tissue damage by ETR antagonism was more substantial in the systems more susceptible to VOCs, e.g., kidneys and lungs, than in less affected vascularized beds, e.g., limbs or the lower mesenteric artery (not shown).

Dense rbcs with an abnormally high HbS concentration (due to loss of K^+, Cl^-, and water from the cells) are a prominent feature of SCD. The extreme dependence of polymerization kinetics on HbS concentration means that these dehydrated rbcs rapidly sickle when deoxygenated. Blockade of K^+ loss from the rbc prevents the increase in HbS concentration and reduces rbc sickling. Two ion transport pathways — the K-Cl cotransporter (44) and the Gardos channel (KCa3.1) — play prominent roles in the dehydration of sickle rbcs (45). The Gardos channel has been linked to the endothelin type B receptor (ETB) in normal and sickle rbcs (21). It has been shown to be activated in vitro by a high concentration of exogenous ET-1. Our findings confirm these observations in rbcs isolated from normal and SAD mice and provide evidence for ETR-mediated regulation of rbc density in vivo, consistent with recent data

obtained with a specific ETB antagonist (22). However, the kinetics of the regulation of rbc hydration and K^+ content in vivo are slow (several hours) relative to the hemodynamic and antiinflammatory effects of bosentan in this model, which are rapid. This suggests that regulation of rbc hydration and K^+ content is of minor importance in the experimental therapeutic action of bosentan.

Increased activation and adhesion of leukocytes and, in particular, neutrophils play important roles in the clinical manifestations of SCD. It has been shown in another model of sickle-cell VOCs that human leukocytes adhering to the vessel wall can directly contribute to vascular occlusion in the cremaster muscle of mice through interactions with sickle rbcs. Nearly all patients with SCD have abnormally high leukocyte counts, and epidemiological data indicate that the higher the leukocyte count, the worse the prognosis (26, 46). Additionally, acute VOCs and acute chest syndrome are associated with high leukocyte and neutrophil counts (33). Furthermore, other reports of rapid onset of painful crises, acute chest syndrome, and death after administration of G-CSF or GM-CSF (47–49) suggest that leukocytes and neutrophils are directly involved in the pathophysiology of SCD. Both leukocytes and endothelial cells carry functional ETRs. ET-1 changes rabbit neutrophil deformability and CD11b production in a dose-dependent fashion, leading to increased neutrophil sequestration in pulmonary microvessels (50). ET-1 is produced by activated endothelial cells (4), but may also be produced by macrophages (36), thereby increasing vasoconstriction and inflammation. There are no comprehensive studies on the action of ETRs in SCD. However, our findings indicate that preventive ETR antagonism substantially inhibits acute VOC-induced increases in peripheral neutrophil counts, total leukocyte counts, and neutrophil infiltration of the bronchoalveolar space, renal and pulmonary MPO activity, and peroxynitrite-induced tissue damage. The antiinflammatory action of ETR antagonism may be direct or indirect through protective effects against ischemia-induced tissue damage and leukocyte recruitment. It would be valuable to investigate the roles of ETR in the mechanism of SCD-dependent vascular inflammation. If bosentan proves safe and effective for preventing or treating acute vasoocclusive events in the clinical setting, it may provide major benefits for lung and renal integrity, quality of life, and survival of sickle-cell patients.

Methods

Animal model

Animals were used in accordance with the NIH *Guide for the care and use of laboratory animals* (NIH publication no. 85-23. Revised 1985), and the study protocol was approved by Services Vétérinaires de la Santé et de la Production Animale, Ministère de l'Agriculture (Paris, France).

SAD1 (SAD) $Hbb^{single/single}$ hemizygous mice (18) were used in this study. This strain harbors a recombinant h^{β}-globin gene construct expressing human hemoglobin SAD ($\alpha 2\beta 2^{SAD}$), which contains 2 mutations (Antilles [β^{23I}] and D Punjab [β^{121Q}]) in addition to the β^{S6V} mutation. These 2 additional mutations result in an increase in polymer formation in the presence of mouse hemoglobin. This mouse model of SCD is lethal in utero in the homozygous state, but the hemizygous genotype has a mild SCD with reduced survival, priapism (51), and kidney defects (18, 51) that are typical of SCD. This strain is bred on the C57BL/6J genetic background (> 12 backcrosses).

H/R model for acute sickle-cell vasoocclusive events

The experimental setting has been described previously (20). Congenic C57BL/6J transgenic SAD mice and littermates were used. Control and SAD mice were divided into 8 groups of 6 to 12 mice each. Four groups were kept under steady state conditions (normoxia), and the other groups were exposed to hypoxia (8% O_2) for 18 or 46 hours followed by 2 hours normoxia. In another set of experiments, WT and SAD mice were exposed to 10% O_2, and the O_2 concentration was reduced to 6% over 2 hours; the mice were then maintained in 6% O_2 for 10 hours.

The ETRA

In acute experiments, isoflurane-anesthetized mice were infused with the dual endothelin receptor antagonist bosentan (sodium salt, RO-47-0203/001; 20 mg/kg) in 100 μl of 0.9% saline through the retroorbital sinus. Vehicle (0.9% saline) or 20 mg/kg of the calcium channel blocker nicardipine were i.v. injected as controls. In chronic experiments, bosentan or Tracleer was mixed with powdered food supplied to the animals at an active dose of 100 mg/kg/d for 14 days (this dose was chosen based on the findings of preliminary pharmacokinetic studies). Bosentan was provided by Actelion.

Real-time RT-PCR and in situ hybridization analysis of preproET-1 mRNA

PreproET-1 mRNA in tissues was assayed by real-time RT-PCR. Total RNA was extracted from samples of one-fourth of a kidney by the TriZOL method and reverse transcribed with SuperScript II (Invitrogen). The QuantiTect SYBR Green PCR Kit (QIAGEN) was used to amplify cDNA for 40 cycles on an ABI PRISM 7000 thermal cycler.

The 18S reference primer sequences were 5′-GAGCGAAAGCATTTGCCAAG-3′ and 5′-GGCATCGTTTATGGTCGGAA-3′. *PreproET-1* was amplified with the primers 5′-TTCCCGTGATCTTCTCTCTGC-3′ and 5′-CTGCACTCCATTCTCAGCTCC-3′. Amplification products were compared with a range of *preproET-1* and 18S amplicons from normal kidney cDNA. A mouse *preproET-1* probe was generated from lung cDNA by PCR with 5′-ATCAGAGCGACCAGACACCG-3′ and 5′-ATGTGCTCGGTTGTGCGTCA-3′ oligonucleotides. This 707-bp fragment was inserted into pGEM-T (Promega). Probes were labeled by in vitro transcription, and in situ hybridization was performed as previously described (52).

Noninvasive ultrasound study of cardiac and renal hemodynamics

Ultrasound examination was carried out under light anesthesia, such that mice could be restrained without ligature.

Anesthesia. Isoflurane (0.75% isoflurane in 100% O_2) was administered through a vaporizer (model 100-F; Ohio Medical Instruments). Isoflurane induction was performed by the same individual over a 2-minute period in an isolation chamber and anesthesia was maintained by spontaneous breathing of the same mixture at a flow rate of 5 l/min through a small nose cone. A small plastic bag surrounding the nose cone was attached to wall suction and used to scavenge excess gas. The gas mixture with 0.75% isoflurane was sufficient to obtain sedation without substantial cardiorespiratory depression. We used an echocardiograph (Vivid 7; GE Medical Systems ultrasound) equipped with a 12-MHz linear transducer (12L). Data were transferred online to an ultrasound image workstation for subsequent analysis (PC EchoPAC; GE Medical Systems ultrasound).

Preparation for imaging. After sedation, the mice were shaved to improve probe contact and then placed in the decubitus position. The ultrasound device was placed on the left side of the abdomen for ultrasound analysis of the kidneys. The mice were then placed in the left lateral decubitus position and the ultrasound device placed on the anterior part of the chest for CO acquisition. Placing the transducer in these positions avoided putting pressure on the abdomen and chest, as pressure alone may cause bradycardia and hypotension. The mice were laid on a heating blanket (38°C) to avoid hypothermia induced by anesthesia affecting cardiac function and heart rate.

Measurements of kidney size and blood flow velocity in the renal arteries. Two-dimensional ultrasound imaging was used to measure kidney sizes. A left-sided longitudinal B-mode image of the abdomen showed the aorta between the 2 renal arteries, allowing measurements of the width and the height of the right and left kidneys; the transducer was slightly displaced from one kidney to the other. Imaging depth was set at 2 to 3 cm when the zoom was used, and the frame rate was approximately 50 frames/s. Color Doppler mode was activated and the renal arteries were drawn and localized on the screen by their color-coded blood flow. The configuration selected for color Doppler ultrasound acquisition involved a frequency emission of 6.7 MHz, a pulsed repetition frequency set at 3.5 kHz, a frame rate of 37.8 frames/s, and a low velocity rejection of 1.65 cm/s. A pulsed Doppler sample gate was placed on the longitudinal axis of the right renal artery as close as possible to the emergence of the aorta, and the pulsed Doppler spectrum was recorded. The configuration used for Doppler ultrasound acquisition was a frequency emission of 6.7 MHz, a pulsed repetition frequency set between 4.3 and 10.8 kHz, a sample volume of 1 mm^3, and a low velocity rejection of 0.6 cm/s. The minimum detectable velocity was about 1 cm/s and the maximum between 50 and 125 cm/s, consistent with blood flow in peripheral arterial vessels. The ultrasound beam width of the pulsed Doppler was small enough (1.1 mm) to ensure that flow from neighboring vessels did not interfere with measurements focused on the renal artery. Indeed, neighboring vessels of the mesenteric artery were not localized by color Doppler ultrasound; the distance between the 2 arteries was larger than the volume of measurement of the Doppler sample. Peak systolic and end-diastolic blood-flow volume (BFV) waveforms were measured from the pulsed Doppler spectrum of the renal artery by placing calipers on the screen. Time-averaged mean BFV was measured by redrawing the blue line drawn on the Doppler spectrum. BFV was measured with correction of the angle between the long axis of each vessel and the Doppler beam. The steering mode of the Doppler beam helped to avoid the need to use angle correction greater than 10°. Kidney size and BFV were measured by the same investigator, and the mean of 3 measurements was used for calculations.

Two series of paired measurements separated by 2-minute intervals were compared, and the relative (positive or negative) differences (Di) between each pair of measures were calculated. The agreement between these 2 measurements was estimated as the mean and the SD of the Di. Repeatability of BFV measurements was investigated in 25 mice by calculation of the repeatability coefficient (RC) with the following formula: $RC^2 = \Sigma Di^2/N$, where N is the sample size. This coefficient is the SD of the estimated difference between 2 repeated measurements. The RC values for intraobserver repeatability were 110 to 120 μm for the height and width of the kidneys, 1.5 cm/s for the systolic BFV, 1.7 cm/s for the end-diastolic BFV, and 1.7 cm/s for the mean BFV for the right renal artery; these values were not significantly different from zero.

Calculation of CO. A parasternal long-axis B-mode image of the chest allowed measurement of the pulmonary artery diameter. The imaging depth was set at 1.5 to 2 cm when the zoom was used, and frame rate was 49.5 frames/s. A pulsed Doppler sample was then placed on the longitudinal axis of the pulmonary artery and the spatial flow profile recorded. The configuration used for Doppler ultrasound acquisition involved a frequency emission of 6.7 MHz, a pulsed repetition frequency set at 10.5 kHz, a sample volume of 1 mm^3, and a low velocity rejection of 0.6 cm/s. The minimum detectable velocity was about 1 cm/s, and the maximum was 120 cm/s. Time-averaged mean BFV was measured from the pulsed Doppler spectrum by redrawing the blue line drawn on the Doppler spectrum. BFV was measured with correction of the angle between the long axis of each vessel and the Doppler beam. The steering mode of the Doppler beam helped to avoid having to use an angle correction greater than 10°. CO was calculated with the following formula: $CO = [(Vmean \times 60)(\pi \times (Dpa/2)^2)]$, where CO is expressed in ml/min, *Vmean* is the time-averaged mean BFV in cm/s, and *Dpa* is the pulmonary artery diameter in cm.

The RC values for intraobserver repeatability were 110 to 120 μm for the pulmonary artery diameter, 4 cm/s for the systolic BFV, and 1.9 cm/s for the mean BFV in the pulmonary artery; these values were significantly different from zero. Moreover, this noninvasive approach was compared with an invasive in situ measurement of renal blood flow (Supplemental Methods and Supplemental Figure 3).

Histopathology and immunochemistry

All mice were dissected, and samples of bone marrow, spleen, lung, and kidney were collected from all animals. Each organ was cut into 2 parts, one being immediately frozen in liquid nitrogen and the other fixed in formalin and embedded in paraffin. Multiple (at least 5) 3-μm whole-mount sections were obtained from each paraffin-embedded organ sample and were stained with H&E, Masson trichrome, and May-Grünwald-Giemsa. Two pathologists independently and blindly evaluated the tissue architecture and changes for WT mice under hypoxia and SAD mice under hypoxia with or without bosentan. The pathological criteria for quantification of the changes in vessels were as previously described (20). Tissue abnormalities in SAD mice exposed to H/R-sickled rbcs were visible in fixed sections of bone marrow and spleen. Microvascular occlusions and secondary end-organ pathology were observed in the spleen, lung, kidney, and liver of Hb SAD mice. The pathological findings detected included congestive splenomegaly, pulmonary congestion with hemorrhage, thrombosis and fibrosis, renal vascular congestion, extramedullary hematopoiesis in the liver, systemic hemosiderosis, and priapism.

Lungs were removed from mice; one lung was immediately frozen in liquid nitrogen and the other was fixed in formalin and embedded in paraffin. At least five 3-μm whole-mount sections were obtained from each paraffin-embedded lung and were stained with H&E, Masson trichrome, and May-Grünwald-Giemsa. Two pathologists independently and blindly assessed tissue architecture and changes in WT mice under hypoxia and SAD mice under hypoxia with or without bosentan treatment. The pathological criteria used for quantification of the changes in vessels and bronchi have been described previously (20). Bronchoalveolar lavage fluids were collected by instilling and withdrawing 5 ml of sterile PBS 4 times through an intratracheal cannula. Cells were recovered by centrifugation and counted by microcytometry. The percentage of neutrophils was determined after cytospin centrifugation, fixation, and staining (20). Microvascular congestion of formalin-fixed, paraffin-embedded kidneys was assessed after Masson trichrome staining. Glomerular tufts of at least 20 glomeruli per mouse were manually defined. Glomeruli were randomly selected in a series of images of the renal cortex. To ensure that similar positions in the different animals were analyzed, the outer edge of each square wide field (acquired with a ×20 objective and DP70 Olympus digital camera) was systematically set tangent to the renal capsule in sagittal sections of the kidneys; thus, equivalent proportions of superficial and deep glomeruli were studied in each condition. High signal-to-background epifluorescence emanating specifically from rbcs was obtained by illuminating Masson trichrome–stained sections and collecting emitted fluorescence through a standard fluorescent filter for rhodamine (Olympus). The rbc relative area was measured by image analysis with ImageJ software (NIH) after thresholding for the color corresponding to entrapped rbcs. A different pathologist blind to the experimental conditions evaluated the proportion of congested glomeruli by counting the number of congested and noncongested glomeruli among 50 glomeruli/Masson trichrome–stained kidney section. Staining for nitrotyrosine was carried out with a rabbit anti-nitrotyrosine IgG (Upstate) and processed in a NexES IHC automated immunohistochemistry slide-staining system (Ventana).

Hematological parameters and immunoblot analysis

The hematological parameters were measured as described previously (18, 19). Density distribution curves were obtained according to the method of Danon and Marikovsky (18, 19). Density values defined in relationship to the most dense 20% of cells (D20) were determined for each curve. The remaining cells were washed 4 more times with choline washing solution (172 mM choline chloride, 1 mM $MgCl_2$, and 10 mM Tris-MOPS, pH 7.4 at 4°C) for measurement of internal Na^+ and K^+ content by atomic absorption spectrometry.

Endothelin B receptor protein was assayed by immunoblot analysis using specific antibody against endothelin B receptor (Capralogics Inc.) in red cells prepared as previously described (53); anti-actin (Sigma-Aldrich) was used as the loading control.

MPO activity assay

MPO is abundant in neutrophils and was assessed as an index of activation of neutrophils in kidneys and lungs. MPO acts as a hydrogen peroxide (H_2O_2) oxidoreductase. MPO activity was measured as described previously with modifications (54). Frozen kidney samples were homogenized twice in a hexadecyltrimethylammonium bromide (HDTB) buffer (13.7 mM HDTB with 50 mM K^+phosphate buffer, pH 6) (Sigma-Aldrich). The samples were centrifuged for 1 hour at 14,000 *g*, and the supernatant was collected and stored at –20°C. The reaction buffer was 50 mM KH_2PO_4 at pH 6 with 0.68 mM O-dianisidine and 29 mM H_2O_2. MPO catalyzed the production of oxygen radicals (O^-) and water from the H_2O_2 in the buffer. The oxygen radical combined with O-dianisidine dihydrochloride, which was converted to a colored compound and its absorbance measured with a spectrophotometer at 460 nm. MPO activity was measured over a period of 15 minutes and was expressed in OD/min/mg protein.

Statistics

A 2-way ANOVA followed by 2-tailed Fisher's exact test was used to compare various measurements (body weight, heart rate, CO, peak systolic BFV, end-diastolic BFV, and mean BFV in the renal arteries) in SAD mice with those in the control group before and after hypoxic exposure. The 2-tailed Wilcoxon's matched-pair signed-rank test was used to evaluate the effect of acute infusion of bosentan in each individual mouse. Nonparametric Kruskal-Wallis ANOVA and analysis by the 2-tailed Mann-Whitney test were used for other cases.

Survival curves were calculated according to the Mantel-Haenszel method with Prism software (GraphPad). Results are expressed as means ± SEM. A *P* value of less than 0.05 was considered statistically significant.

Acknowledgments

We thank the Société Française d'Hypertension Artérielle and the Société Française d'Hématologie for funding Nathalie Sabaa and the joint Assistance Publique-Hôpitaux de Paris — INSERM Contrat d'Interface for funding Pierre-Louis Tharaux. We thank Martine Clozel and Marc Iglarz for providing bosentan.

Received for publication July 18, 2007, and accepted in revised form February 6, 2008.

Address correspondence to: Pierre-Louis Tharaux, INSERM, Unit 689, Cardiovascular Research Center Lariboisière, 141 Boulevard de la Chapelle, Paris F-75010, France. Phone: 33-615-95-53-67; Fax: 33-14-81-31-28; E-mail: tharaux@chusa.jussieu.fr.

Nathalie Sabaa and Lucia de Franceschi contributed equally to this work.

1. Hebbel, R.P., Osarogiagbon, R., and Kaul, D. 2004. The endothelial biology of sickle cell disease: inflammation and a chronic vasculopathy. *Microcirculation.* **11**:129–151.
2. Turhan, A., Weiss, L.A., Mohandas, N., Coller, B.S., and Frenette, P.S. 2002. Primary role for adherent leukocytes in sickle cell vascular occlusion: a new paradigm. *Proc. Natl. Acad. Sci. U. S. A.* **99**:3047–3051.
3. Yanagisawa, M., et al. 1988. A novel potent vasoconstrictor peptide produced by vascular endothelial cells. *Nature.* **332**:411–415.
4. Phelan, M., Perrine, S.P., Brauer, M., and Faller, D.V. 1995. Sickle erythrocytes, after sickling, regulate the expression of the endothelin-1 gene and protein in human endothelial cells in culture. *J. Clin. Invest.* **96**:1145–1151.
5. Firth, J., and Ratcliffe, J. 1992. Organ distribution of the three rat endothelin messengers RNAs and the effects of ischemia on renal gene expression. *J. Clin. Invest.* **90**:1023–1031.
6. Tharaux, P.L., et al. 1999. Vascular endothelin-1 gene expression and synthesis and effect on renal type I collagen synthesis and nephroangiosclerosis during nitric oxide synthase inhibition in rats. *Circulation.* **99**:2185–2191.
7. Hammerman, S.I., et al. 1997. Endothelin-1 production during the acute chest syndrome in sickle cell disease. *Am. J. Respir. Crit. Care Med.* **156**:280–285.
8. Rybicki, A.C., and Benjamin, L.J. 1998. Increased levels of endothelin-1 in plasma of sickle cell anemia patients. *Blood.* **92**:2594–2596.
9. Werdehoff, S.G., Moore, R.B., Hoff, C.J., Fillingim, E., and Hackman, A.M. 1998. Elevated plasma endothelin-1 levels in sickle cell anemia: relationships to oxygen saturation and left ventricular hypertrophy. *Am. J. Hematol.* **58**:195–199.
10. Tharaux, P.L., et al. 2005. Urinary endothelin-1 as a marker of renal damage in sickle cell disease. *Nephrol. Dial. Transplant.* **20**:2408–2413.
11. de Jong, P.E., and Statius van Eps, L.W. 1985. Sickle cell nephropathy: new insights into its pathophysiology. *Kidney Int.* **27**:711–717.
12. Brezis, M., and Rosen, S. 1995. Hypoxia of the renal medulla--its implications for disease. *N. Engl. J. Med.* **332**:647–655.
13. Platt, O.S. 2000. The acute chest syndrome of sickle cell disease. *N. Engl. J. Med.* **342**:1904–1907.
14. Epstein, F.H. 1997. Oxygen and renal metabolism. *Kidney Int.* **51**:381–385.
15. Saborio, P., and Scheinman, J.I. 1999. Sickle cell nephropathy. *J. Am. Soc. Nephrol.* **10**:187–192.
16. Machado, R.F., et al. 2007. Severity of pulmonary hypertension during vaso-occlusive pain crisis and exercise in patients with sickle cell disease. *Br. J. Haematol.* **136**:319–325.
17. Clozel, M., et al. 1994. Pharmacological characterization of bosentan, a new potent orally active nonpeptide endothelin receptor antagonist. *J. Pharmacol. Exp. Ther.* **270**:228–235.
18. Trudel, M., et al. 1991. Towards a transgenic mouse model of sickle cell disease: hemoglobin SAD. *EMBO J.* **10**:3157–3165.
19. De Franceschi, L., Brugnara, C., Rouyer-Fessard, P., Jouault, H., and Beuzard, Y. 1999. Formation of dense erythrocytes in SAD mice exposed to chronic hypoxia: evaluation of different therapeutic regimens and of a combination of oral clotrimazole and magnesium therapies. *Blood.* **94**:4307–4313.
20. de Franceschi, L., et al. 2003. Inhaled nitric oxide protects transgenic SAD mice from sickle cell disease-specific lung injury induced by hypoxia/reoxygenation. *Blood.* **102**:1087–1096.
21. Rivera, A., Jarolim, P., and Brugnara, C. 2002. Modulation of Gardos channel activity by cytokines in sickle erythrocytes. *Blood.* **99**:357–603.
22. Rivera, A. 2007. Reduced sickle erythrocyte dehydration in vivo by endothelin-1 receptor antagonists. *Am. J. Physiol. Cell Physiol.* **293**:C960–C966.
23. Rivera, A., Rotter, M.A., and Brugnara, C. 1999. Endothelins activate Ca(2+)-gated K(+) channels via endothelin B receptors in CD-1 mouse erythrocytes. *Am. J. Physiol.* **277**:C746–C754.
24. Nath, K.A., et al. 2005. Transgenic sickle mice are markedly sensitive to renal ischemia-reperfusion injury. *Am. J. Pathol.* **166**:963–972.
25. Vogler, C., et al. 1996. Microangiopathic glomerulopathy in children with sickle cell anemia. *Pediatr. Pathol. Lab. Med.* **16**:275–284.
26. Miller, S.T., et al. 2000. Prediction of adverse outcomes in children with sickle cell disease. *N. Engl. J. Med.* **342**:83–89.
27. Lopez Farre, A., et al. 1993. Effect of endothelin-1 on neutrophil adhesion to endothelial cells and perfused heart. *Circulation.* **88**:1166–1171.
28. Kaul, D.K., and Hebbel, R.P. 2000. Hypoxia/reoxygenation causes inflammatory response in transgenic sickle mice but not in normal mice. *J. Clin. Invest.* **106**:411–420.
29. Kirsch, M., and de Groot, H. 2002. Formation of peroxynitrite from reaction of nitroxyl anion with molecular oxygen. *J. Biol. Chem.* **277**:13379–13388.
30. Prutz, W.A., Monig, H., Butler, J., and Land, E.J. 1985. Reactions of nitrogen dioxide in aqueous model systems: oxidation of tyrosine units in peptides and proteins. *Arch. Biochem. Biophys.* **243**:125–134.
31. Bank, N., et al. 1998. Peroxynitrite formation and apoptosis in transgenic sickle cell mouse kidneys. *Kidney Int.* **54**:1520–1528.
32. Aslan, M., et al. 2003. Nitric oxide-dependent generation of reactive species in sickle cell disease. Actin tyrosine induces defective cytoskeletal polymerization. *J. Biol. Chem.* **278**:4194–4204.
33. Vichinsky, E.P., et al. 2000. Causes and outcomes of the acute chest syndrome in sickle cell disease. National Acute Chest Syndrome Study Group. *N. Engl. J. Med.* **342**:1855–1865.

34. Powars, D.R., Chan, L.S., Hiti, A., Ramicone, E., and Johnson, C. 2005. Outcome of sickle cell anemia: a 4-decade observational study of 1056 patients. *Medicine (Baltimore).* **84**:363–376.
35. Guasch, A., Navarrete, J., Nass, K., and Zayas, C.F. 2006. Glomerular involvement in adults with sickle cell hemoglobinopathies: Prevalence and clinical correlates of progressive renal failure. *J. Am. Soc. Nephrol.* **17**:2228–2235.
36. Ehrenreich, H., et al. 1990. Endothelins, peptides with potent vasoactive properties, are produced by human macrophages. *J. Exp. Med.* **172**:1741–1748.
37. Kourembanas, S., McQuillan, L.P., Leung, G.K., and Faller, D.V. 1993. Nitric oxide regulates the expression of vasoconstrictors and growth factors by vascular endothelium under both normoxia and hypoxia. *J. Clin. Invest.* **92**:99–104.
38. Gladwin, M.T., et al. 2003. Divergent nitric oxide bioavailability in men and women with sickle cell disease. *Circulation.* **107**:271–278.
39. Reiter, C.D., et al. 2002. Cell-free hemoglobin limits nitric oxide bioavailability in sickle-cell disease. *Nat. Med.* **8**:1383–1389.
40. Aslan, M., et al. 2001. Oxygen radical inhibition of nitric oxide-dependent vascular function in sickle cell disease. *Proc. Natl. Acad. Sci. U. S. A.* **98**:15215–15220.
41. Boulanger, C., and Luscher, T.F. 1990. Release of endothelin from the porcine aorta. Inhibition by endothelium- derived nitric oxide. *J. Clin. Invest.* **85**:587–590.
42. Ito, S., Juncos, L.A., Nushiro, N., Johnson, C.S., and Carretero, O.A. 1991. Endothelium-derived relaxing factor modulates endothelin action in afferent arterioles. *Hypertension.* **17**:1052–1056.
43. de Franceschi, L., et al. 2006. Protective effects of S-nitrosoalbumin on lung injury induced by hypoxia-reoxygenation in mouse model of sickle cell disease. *Am. J. Physiol. Lung Cell Mol. Physiol.* **291**:L457–L465.
44. Rust, M.B., et al. 2007. Disruption of erythroid K-Cl cotransporters alters erythrocyte volume and partially rescues erythrocyte dehydration in SAD mice. *J. Clin. Invest.* **117**:1708–1717.
45. Brugnara, C., De Franceschi, L., and Beuzard, Y. 2001. Erythrocyte-active agents and treatment of sickle cell disease. *Semin. Hematol.* **38**:324–332.
46. Platt, O.S., et al. 1994. Mortality in sickle cell disease. Life expectancy and risk factors for early death. *N. Engl. J. Med.* **330**:1639–1644.
47. Pieters, R.C., Rojer, R.A., Saleh, A.W., Saleh, A.E., and Duits, A.J. 1995. Molgramostim to treat SS-sickle cell leg ulcers. *Lancet.* **345**:528.
48. Abboud, M., Laver, J., and Blau, C.A. 1998. Granulocytosis causing sickle-cell crisis. *Lancet.* **351**:959.
49. Adler, B.K., et al. 2001. Fatal sickle cell crisis after granulocyte colony-stimulating factor administration. *Blood.* **97**:3313–3314.
50. Sato, Y., Hogg, J.C., English, D., and van Eeden, S.F. 2000. Endothelin-1 changes polymorphonuclear leukocytes' deformability and CD11b expression and promotes their retention in the lung. *Am. J. Respir. Cell Mol. Biol.* **23**:404–410.
51. De Paepe, M.E., and Trudel, M. 1994. The transgenic SAD mouse: a model of human sickle cell glomerulopathy. *Kidney Int.* **46**:1337–1345.
52. Le Jan, S., et al. 2003. Angiopoietin-like 4 is a proangiogenic factor produced during ischemia and in conventional renal cell carcinoma. *Am. J. Pathol.* **162**:1521–1528.
53. Franceschi, L.D., et al. 2006. Regulation of K-Cl cotransport by protein phosphatase 1alpha in mouse erythrocytes. *Pflugers Arch.* **451**:760–768.
54. Melnikov, V.Y., et al. 2001. Impaired IL-18 processing protects caspase-1-deficient mice from ischemic acute renal failure. *J. Clin. Invest.* **107**:1145–1152.